Analysis of the long-term drift rates and oscillations of Jupiter's largest vortices

R. Morales-Juberías[1]

Physics Department

New Mexico Tech, Socorro NM 87801

rmjuberias@gmail.com

A. A. Simon [2]

NASA Goddard Space Flight Center Solar System Exploration Division

8800 Greenbelt Road Greenbelt, MD 20771 USA

Amy.simon@nasa.gov

R. Cosentino [3]

University of Maryland College Park & Goddard Space Flight Center

8800 Greenbelt Road Greenbelt, MD 20771 USA

richard.cosentino@nasa.gov

Received _____; accepted _____

To appear in Icarus

ABSTRACT

Jupiter's troposphere is dynamically characterized by a series of alternating eastward and westward jets. Embedded between these alternating jets, large vortices, characterized by their high speed closed circulations can be found in several latitudinal bands. The Great Red Spot (GRS) and the White Ovals (WOS) located at ≈ 22 and ≈ 30 degrees south respectively[1] are the largest of these vortices. The GRS has undergone significant changes in size, coloration and **maximum circumferential wind speed** over the last two decades. The three WOS also experienced changes in size, and **they merged over time until there was only one remaining, which since then has been formally known as oval BA**. Here we used **over four decades worth of** data from the Database for Object Positions on Jupiter (JUPOS), to investigate the long-term mean longitudinal drift of these largest vortices, and to characterize the deviations from this mean drift. A linear fit to the GRS drift speed for the last two decades gives a rate of change of $(3.1\pm0.4)^{-3}\,^\circ$/day/year. For oval BA we find that **its annual drift rate changed from $-0.39\,^\circ$/day in 2016 to $-0.58\,^\circ$/day in 2020 following a steep trend that is best fitted by a second order polynomial.** Regarding oscillations, we find that for the last two decades the GRS has continued to oscillate longitudinally with the same period (90 days) and peak-to-peak amplitude (1.2 degrees **longitude**) as reported historically. **For the WOS, the data prior to 2000 seems to indicate that they presented similar oscillations with periods of ≈ 158 days and peak-to-peak amplitudes of ≈ 1.6 degrees. The analysis of the data for oval BA since the year 2000 reveals evidence of an oscillation with a period of ≈ 138 days and peak-to-peak amplitude of ≈ 1.6 degrees longitude.**

[1]Latitudes are planetographic unless otherwise noted

Subject headings: Jupiter; Jupiter, atmosphere; Atmospheres, dynamics

1. Introduction

With a volumetric mean radius of 69,911 km [2], Jupiter is the largest planet in the solar system. Its large angular size in the sky (between 30" to 47" depending on its relative position to Earth) makes it a great target for detailed observations even with modest telescopes (Kardasis et al. 2016). Small aperture telescopes can capture the general banded appearance of the planet as well as the location of its major storms like the Great Red Spot (GRS) and the White Ovals (WOS). Using image stacking, amateurs can achieve enough resolution to clearly distinguish details in these largest features of the planet. Figure 1 shows comparatively how Jupiter looks like through a 100 cm F/8 telescope located in Chile using image stacking and through the Hubble Space Telescope (HST). In this paper, we extracted information about the location of these spots from the 45,482 observational records in the JUPOS database (Figure 2) to investigate their long-term drift rates and to analyze their oscillatory behavior.

Jupiter's GRS is the largest vortex on the planet. Located at a latitude of ≈ 22 degrees south, it is believed to be at least 150 years old. The first reports about the existence of the GRS described it as an elongated oval with a length of 34° and a width of 10° (Denning 1885). During the 1970s and 1980s, the average reported size of the spot was $21° \times 12°$ (Peek 1958; Rogers 1995). Over the last few decades, the GRS has continued reducing in size while also changing its appearance and maximum circumferential wind speed (Simon-Miller et al. 2002; Simon et al. 2018). It is also known that the GRS shows longitudinal oscillations. Solberg (1969) and Reese (1972) analyzed photographic plates taken in the 1960s and showed that the longitudinal position of the GRS oscillated with a period of 89.89 days and a peak-to-peak amplitude of about 1.54 degrees. Guitar (1984) remeasured some of the 1960s plates and extended the analysis to cover a time span of 20

[2]See appendix A for details about Jupiter Radii and latitude systems

years from 1961 to 1981. He found a similar oscillation period of 89.93 days with a slightly smaller amplitude of about 1.06 degrees. Trigo-Rodriguez et al. (2000) again confirmed the longitudinal oscillations of the GRS based on an analysis of CCD images taken between the years 1993 and 1999. During this time span, they reported an average oscillation period of 89.8 days with an amplitude of about 1.2 degrees. **Finally,** Rogers (2008) **also showed how the 90 day period remained constant from 2002 to 2006, based on analysis of data in the JUPOS database.**

The WOS are Jupiter's second largest vortices. They were located at about 33 degrees south in the latitudinal band south of the GRS. The WOS formed in 1938 when the South Temperate Belt clouded over and then pinched off at six different longitudinal locations that were labeled in alphabetical order A, B, C, D, E, and F (Rogers 1995). Over time these locations started to move towards each order while showing evidence of recirculation between them, **thus forming the ovals that would become known as BC, DE and FA.** Originally, much like the GRS, these vortices were elongated in the longitudinal direction, spanning as **wide** as 80 degrees, but over time their longitudinal size became smaller and smaller until their aspect ratio **fell to** ≈ 0.9 (Morales-Juberías et al. 2002). From 1940 to 1998, the three WOS moved relative to each other in the same latitude circle, and in several occasions they came in close proximity of each other (Simon and Beebe 1996; Simon et al. 1998). In 1998, as a consequence of one of these close approaches, two of these ovals, BC and DE, merged to form a single storm which became known as oval BE (Sánchez-Lavega et al. 1999). This newly formed storm was similar in form and dynamics to its progenitors and continued drifting in the same latitudinal band together with oval FA. In the year 2000, these two remaining storms BE and FA also merged to form a single storm **which became formally known as** BA (Sanchez-Lavega et al. 2001; Morales-Juberías et al. 2003). None of these mergers could be observed and analyzed in detail because of the close proximity of Jupiter to the Sun when they happened. Since its formation, oval BA

has remained the dominant vortex in its latitude and has experienced different episodes of coloration changes (Simon-Miller et al. 2006; García-Melendo et al. 2009; Pérez-Hoyos et al. 2009; Wong et al. 2011).

Here, we used the data from the JUPOS database to investigate the long-term mean longitudinal drift and to characterize the nature of the deviations from this mean for the GRS and for the WOS for the last four decades of ground-based observations. We also present results concerning the evolution of the latitudinal position and size of these spots derived from the same database, and compare them to the trends derived from higher resolution observations during the same time period.

2. Observations and methodology

In this paper, we analyze the position of the GRS and the WOS reported in the JUPOS database. JUPOS is an amateur astronomical project that collects precise positions of Jovian cloud features, analyzes them in drift charts, and examines if and how their movements change in time. The JUPOS database contains information about the location of the GRS dating back to 1831 based on drawings of the planet, and up to the year 2021 based on CCD images taken largely by amateur astronomers. The database contains 16 fields, namely, the record number, the object code, the region of the planet where the object is located, the date and time of the observation, the Julian date, the longitude of the feature in the three systems of longitude that exist for Jupiter (SI, SII and SIII) [3], the latitude of the feature (planetographic), the measurement type, the channel or filter used, the instrument used, the magnification, the image orientation and finally the observer name (Hans Jorg Mettig and Grischa Hahn 1995). The advantage of using this database

[3]See appendix B for details about the different systems of longitude

is the sheer number of high quality observations, often obtained by stacking hundreds to thousands of video frames to produce high-resolution images. Given the frequency of observations, small deviations in motion can be discerned, and uncertainties are reduced by having reports from multiple observers around the world.

In order to process and analyze the data in this database, we used Python's package pandas (Wes McKinney 2010; Reback J. & The pandas development team 2020). This allowed us to select and manipulate the data in the database that was relevant to our analysis. To calculate the mean annual drift rate of each spot, first we selected the data corresponding to each spot center as a function of time. The center of each feature is recorded with different codes in the database depending on the precision of the measurement (Hans Jorg Mettig and Grischa Hahn 1995). We selected only the data corresponding to the best precision for our analysis. In Figure 2 we show the data contained on the database for the centers of the GRS and the WOS in System II from year 1960 to 2021. We selected System II for our analysis because historically this is the system of reference associated with the average translation of the GRS.

To determine the annual mean drift rate of each feature we performed a linear fit to the center position in SII per year. For the GRS data this is straightforward, since its position stays within the range from 0 to 360 degrees in System II for this time period. For the WOS data, we had to correct for the domain boundary (zero longitude) crossings before performing the linear fits. In Figure 3 we show the calculated annual mean drift rates for the GRS and the WOS derived from the data shown in Figure 2.

After estimating the annual mean drift rate for each spot, in order to determine the period of oscillations in longitude of the GRS and the WOS, the linear fit was removed for each year. After that, the signal with the residual longitudes was demeaned, and the values for all the different years were concatenated and analyzed using the Lomb-Scargle

method (Lomb 1976; Scargle 1982) to identify the most dominant periods of cyclic changes. The Lomb-Scargle method is particularly well-suited to work with discontinuous and unevenly sampled data series, eliminating the need to fill unevenly spaced time-series with interpolated values. To perform the calculation of the periodogram we used the gastpy package developed by VanderPlas and Ivezić (2015); Vanderplas (2015). Specifically, we use the fast periodogram implementation based on the algorithm developed by Press and Rybicki (1989). In this implementation the normalized periodogram of a data series S_n sampled at nonuniform times t_n is given by:

$$P_{LS}(f) = \frac{1}{2}\left\{\frac{(\sum_n S_n \cos(2\pi f[t_n - \tau]))^2}{\sum_n S_n \cos^2(2\pi f[t_n - \tau])} + \frac{(\sum_n S_n \sin(2\pi f[t_n - \tau]))^2}{\sum_n S_n \sin^2(2\pi f[t_n - \tau])}\right\} \tag{1}$$

where f is the frequency and τ is an offset specified for each frequency to ensure time-shift invariance:

$$\tau = \frac{1}{4\pi f}\tan^{-1}\frac{\sum_n \sin(4\pi f t_n)}{\sum_n \cos(4\pi f t_n)} \tag{2}$$

When written in this form, the expression for the periodogram resembles that of the classical periodogram of evenly sampled data using the Fourier transform. However, the Lomb-Scargle method can also be interpreted in terms of a least-squares fit to a sinusoidal function at each frequency using a least-squares method (VanderPlas 2018).

The precision with which a peak's period (or frequency) can be identified is directly related to the width of the peak, and often the half-width at half-maximum is used. However, as noted in VanderPlas (2018), to first order this value does not depend on either the number of samples or their signal-to-noise ratio. The peak width would be the inverse of the observational baseline, which is somewhat different for all our signals.

In order to quantify the significance of a peak in a periodogram, we calculate the

False-Alarm Probability (FAP) level using the Baluev (2008) method, **since this method produces nearly identical results to the bootstrapping methods but it is computationally more efficient.** The FAP represents the probability that a series with no signal would lead to a peak of similar magnitude, and it gives an estimate of the level that corresponds to a given % false alarm probability for the largest peak, assuming a null hypothesis of non-varying data with Gaussian noise. In our analysis we set this level to be 5%.

Finally, the JUPOS database contains information not only about the center of each feature of interest, but also about its preceding, trailing, northern and southern edges for selected dates. We used this information to look for trends in the EW and NS sizes of the spots for the last two decades and compared these results to higher resolution observations during the same time period as described in the section below.

3. Results

3.1. GRS drift rate, longitudinal oscillations, and size.

The drift rate of the GRS in system II has changed with time from 1970 to 2021, with different periods of acceleration and deceleration. Figure 3 shows the values of the GRS's drift rate per year, derived from the linear fits per year of the data shown in Figure 2. Since the year 2000, there is a clear upward linear trend in the drift rate. A linear fit to the data gives a value for the rate of change of the drift rate during this period of $(3.1 \pm 0.4) \times 10^{-3}\,^{\circ}$/day/year ($R^2 = 0.86$).

In addition to the linear drift described above, the GRS shows evidence of oscillations in longitude as previously reported. When using all the data in the database for the analysis, the signal is affected by the lack of data in some decades. Therefore, we decided to

calculate the power spectra for different temporal windows. The sparse data corresponding to the 1960s and 1970s did not produce statistically significant peaks in the power spectra. The quality, and temporal sampling, of data of the subsequent decades (1980-2010) varied and produced peaks of different significance.

The analysis of the raw data corresponding to the 80s and 90s produces periodograms for which all the peaks are below the 5% FAP level. In order to filter the raw signals, we removed all the points that deviated by δ degrees from the detrended mean. To determine which value of δ produces the most significant peak in each case, we tested values of δ from 2 degrees to 9 degrees and calculate the ratio of the height of highest peak in the periodogram to the false alarm level (FAL). For the series corresponding to the 80s the periodogram peak with the largest height to FAL ratio is found for $\delta = 3$ degrees and it corresponds to a period of 90 days. For the 90s series the peak in the periodogram with the largest height to FAL ratio is found for $\delta = 5$ degrees and it corresponds to a period of 102 days. Even after filtering, the peaks for these two decades are barely statistically significant as shown in Figure 4. **This figure also shows the effect of filtering the 80s and 90s data further using a 5 day exponential moving average (EMA). In this case, the peak in the periodogram with the largest height to FAL ratio for the 80s data is found for $\delta = 8$ degrees, and it corresponds to a period of 111 days. For the 90s series, the most significant peak is again found for a value of $\delta = 5$ and it corresponds to a period of 102. All these results are summarized in Table 1.**

The temporal sampling of the data for the two subsequent decades (2000s, and 2010s) is significantly better than for the previous ones, and the periodogram of the raw detrended longitude data shows peaks that are clearly

above the 5% FAP as shown in Figure 5. The dominant peaks have periods of 90 and 91 days respectively, which in good agreement with previous published results as shown in Table 1. The peaks at ≈ 73 and 117 days seen in the periodogram corresponding to the 2000s, are aliases of the main peak period combined with Jupiter's 399 day synodic period, since the frequencies of these peaks corresponds approximately to the frequency of the main peak plus and minus Jupiter's synodic frequency.

Finally, since the JUPOS database also contains the information about the spot edges for some dates, we used this information to analyze the change in the longitudinal and latitudinal size of the GRS as a function of time. Figure 6 shows the trend of the drift rate, the latitude, and the size of the GRS as a function of time derived from our analysis compared to those recently reported by Simon et al. (2014); Simon et al. (2018). The large error bars in our estimates of the size is due mainly to the difficulty in precisely determining the position of the leading and trailing edge of the spot in a consistent manner by different observers as the spot changes its morphological appearance over time. However, we can see that the overall trend of size vs time follows well the tendency derived from higher resolution observations. For the EW size, a linear fit to the data produces a rate of decrease in size of -0.243 degrees per year ($R^2 = 0.83$). For the NS size it should be noted that in the JUPOS database, the North or South positions of the spots have been recorded just sporadically, which explain the gaps seen in the figure for the NS size of the spot. Consequently, a linear fit to this data is rather poor ($R^2 = 0.34$) but results in a rate of decrease in size of -0.082 degrees per year.

3.2. WOS drift rates, longitudinal oscillations and sizes.

We performed the same analysis described above for the GRS to the data contained in the database pertaining to the WOS. As described in the introduction, before the year 2000 the three White Ovals BC, DE and FA, shared their latitudinal domain and moved relative to each other while interacting with smaller cyclonic vortices embedded between them (Simon et al. 1998). First, we analyzed the longitudinal position data of the WOS in the JUPOS database prior to year 2000 to investigate if it was possible to disentangle any oscillatory behavior other than that caused by the mutual interactions between the spots that eventually led to their mergers (Sánchez-Lavega et al. 1999; Sanchez-Lavega et al. 2001).

3.2.1. Ovals DE and FA

First we present the results corresponding to oval DE. The SII data in the JUPOS database allowed us to estimate the drift rate of this oval from 1967 when the value was $\approx -0.68\,^\circ$/day until 1997 when the mean value was $\approx -0.35\,^\circ$/day. As shown in Figure 3, between those years, the drift rate of oval DE fluctuated between these two values as the WOS moved relative to one another. A linear fit to the data gives a trend of $(11 \pm 1) \times 10^{-3}\,^\circ$/day/year ($R^2 = 0.86$). The analysis of the longitudinal oscillations is not as clean for oval DE as it was for the GRS. **In order to reduce the noise in the signal, before calculating the Lomb-Scargle periodogram, we removed all the points that deviated more than 9 degrees from the detrended mean, since this is produced the largest peak height to FAL ratio in the periodogram. The highest peak found this way corresponded to a period of 159 days. However, its height was still marginally above the FAL. Smoothing the signal with a 5 day exponential moving average had no effect on the period of the peak, but**

increased its significance relative to the FAL. In Figure 7, we show the Lomb-Scargle periodogram corresponding to years 1970-1999 of this filtered signal.

For oval FA, the SII data in the JUPOS database allowed us to estimate the drift rate of the oval FA from 1967 when the value was $\approx -0.64\,^\circ$/day until 2000 when the mean value was $\approx -0.48\,^\circ$/day. Much like oval DE, between those years, the drift rate of oval FA fluctuated between these two values (Figure 3) A linear fit to the data gives a trend of $(7 \pm 1) \times 10^{-3}\,^\circ$/day/year ($R^2 = 0.72$). Similar to the analysis of the longitudinal oscillations for DE, the analysis for FA is quite noisy. We used the same procedure described above to clean the signal before calculating the Lomb-Scargle periodogram. When looking at the dataset between 1970 and 1999, the peak with the largest height to FAL ratio was found when we removed all the points that deviated more than 7 degrees from the detrended mean. The highest peak found this way corresponded to a period of 154 days. However, its height was still marginally above the FAL. Smoothing the signal with a 5 day exponential moving average had no effect on the period of the peak, but increased its significance relative to the FAL. Figure 7 shows the Lomb-Scargle periodogram corresponding to years 1970-1999 of this filtered signal. In addition to the main peak, there is a peak at about 243 days that is close in height to the main peak. The frequency of this peak corresponds approximately to the frequency of the main peak minus Jupiter's synodic frequency, and so this peak is likely an alias of the main peak period combined with Jupiter's 399 day synodic period. The ripples seen around both peaks would be indicative of spectral leaking due to the noise in the signal.

In Table 2 we summarize the results of the spectral analysis of the longitude data corresponding to DE and FA from 1970 to 1999.

3.2.2. Oval BC aka BE aka BA

In the JUPOS database the current oval BA is tracked as a single feature through all its *"identity"* changes. Oval BC, as it was initially known, was tracked from 1967 until 1998. After merging with oval DE, oval BE was tracked from 1998 until its merger with oval FA in the year 2000. From then on, the spot tracked is oval BA.

Interestingly, the mean annual drift rate of the spot tracked continuously shows two clearly separated tendencies that do not match in time with the merger dates (1998 and 2000). From year 1971 until 1990 the annual mean drift rate of the spot decreased in absolute value from $\approx -0.7\,^\circ$/day to $\approx -0.36\,^\circ$/day at a rate of $(18 \pm 3) \times 10^{-3}\,^\circ$/day/year ($R^2 = 0.86$). From year 1990 to 2008, as shown in Figure 8, the trend reverses and the mean annual drift rate increases in absolute value from $\approx -0.36\,^\circ$/day to about $\approx -0.49\,^\circ$/day at a rate of $(6 \pm 1) \times 10^{-3}\,^\circ$/day/year ($R^2 = 0.74$). From year 2008 to 2016 the spot experienced alternating accelerations and decelerations until finally, from 2016 until 2020, it entered a period of very steep increase (in absolute value) of its annual drift rate changing from $-0.39\,^\circ$/day in 2016 to $-0.58\,^\circ$/day in 2020 in a trend that is best fitted by a second order polynomial of the form:

$$\left(\frac{dSII}{dt}\right)_{BA} = -0.0153\,t^2 + 61.697\,t - 62205\ , \tag{3}$$

where SII is the longitude of the spot center in system II and t is the time measured in years.

As it was the case for the data corresponding to ovals DE and FA, the power spectra of the raw detrended data for oval BC/BE during the time period from 1970 to 1999 is quite noisy. We used the same procedure decribed above to filter the signal, and removed all the points that deviated more than

7 degrees from the detrended mean, since this is the value that produced the largest peak height to FAL ratio. The highest peak found this way corresponded to a period of 163 days. However, its height was still marginally above the FAL. Once again, smoothing the signal with a 5 day exponential moving average had no effect on the period of the peak, but increased its significance relative to the FAL. The periodogram corresponding to this detrended signal is shown at the bottom of Figure 7. Once again, the secondary peak shown at ≈ 300 days results from the aliasing of the main peak with Jupiter's synodic period.

The data corresponding to oval BA from 2000 to 2020 was filtered once again to maximize the ratio of the main peak to the FAL by removing the points that deviated by more than 4 degrees from the detrended mean and using a 5-day EMA. The periodogram of this filtered signal reveals a clear dominant peak with a period of 138 days as shown in Figure 9 and Table 2. Other peaks seen in the periodogram (at days 81, 102, 166 and 212 for example) are again aliases of the main peak period and Jupiter's 399 day synodic period. Other large peaks (like those seen at days 156 and 257 for example) could correspond to aliases of the main period with the period between encounters (in longitudinal position) between the GRS and BA which is ≈ 742 days (slightly over 2 years).

Finally, and following the same process applied to the GRS data, we used the information of the positions of the oval BA edges to analyze the change in its longitudinal and latitudinal size. Fig. 10 shows the trend of the drift rate, the latitude, and the size of BA as a function of time. The EW size seems to follow a decreasing trend from 2006 to 2015 with a linear rate of change of -0.453 degrees per year ($R^2 = 0.74$). Since 2015 to 2000, this trend seems to reverse and starts increasing linearly at a rate of $+0.442$ degrees per year ($R^2 = 0.99$). As mentioned

before, since the North or South positions of the spots have been recorded just sporadically in the JUPOS database, the NS size data has even bigger gaps than in the GRS case and the comparison of the variation of the NS size with the EW size is very limited. We filled these gaps in the NS size trend with measurements from images processed and navigated as described elsewhere (Morales-Juberías et al. 2002, 2010; Cosentino et al. 2017). The trends in the changes of the NS size seem to follow the overall trends observed in the EW size. A linear fit to the NS size data between the years 2006 and 2015 results in a rate of change of -0.224 degrees per day ($R^2 = 0.65$). Much like the EW trend, after 2015 the NS trend seems to also reverse and change to 0.154 degrees per year ($R^2 = 0.45$).

4. Discussion

Prior to the year 2000, the details regarding the drift rates and sizes of the GRS and the WOS have been covered by multiple reports Simon and Beebe (1996); Simon et al. (1998); Morales-Juberías et al. (2002); Sánchez-Lavega et al. (1999); Sanchez-Lavega et al. (2001). After 2000, other reports have similarly reported on the evolution of the GRS and oval BA during specific years associated with morphology or coloration changes (Rogers 2008; García-Melendo et al. 2009; Marcus et al. 2012; Sanchez-Lavega et al. 2013; Sánchez-Lavega et al. 2021). Our main interest in investigating the data in the JUPOS database was to determine if it would be possible to detect oscillations in the longitudinal motion of the GRS and the WOS from over four decades worth of much higher cadence amateur data.

4.1. The Great Red Spot

For the GRS, our results seem to indicate that 300 longitude points per decade would be needed in order to obtain statistically significant peaks in the power spectrum. As shown in Table 1 both for the 1980s and the 1990s, the JUPOS database only contained 193 and 210 longitude data points respectively for the GRS. This contrast with the 317 points used by Trigo-Rodriguez et al. (2000) in the 1990s, and would explain why our analysis did not produce statistically significant results for those decades. **Filtering the data to maximize the periodogram peak height to the FAL results in statistically significant peaks that have periods close to the previously reported 90 day period.**

Our periodogram analysis of the longitudinal records of the GRS in the JUPOS database for the two decades from the year 2000 to the year 2020, reveals statistically significant peaks during this period that match the historically reported period and amplitude of 90 days and 1.2 degrees. The power spectra corresponding to the decade of the 2000s has two additional peaks at 73 days and 117 days, **which are aliases of the main peak period combined with Jupiter's 399 day synodic period.**

4.2. The White Ovals

In Table 2 we show the results of our periodogram analysis of the WOS data. **Prior to the year 2000, the WOS could not move in their latitudinal domain as freely as the GRS could in its domain, since they were part of a series of alternating cyclones and anticyclones, usually referred to as a vortex street** (Humphreys and Marcus 2007; Morales-Juberías et al. 2010). **As a consequence, during this time, the spots moved relative to each other prior to their mergers due to running into**

the intervening cyclones embedded among them. Initially, we thought that these interactions would likely veil any potential natural oscillation that a spot placed at this latitude could exhibit. However, the spectral analysis of the detrended and filtered longitudinal positions of these spots prior to their mergers, reveal oscillation periods of about 158 days and peak-to-peak oscillation amplitudes of about 1.6 degrees.

After the year 2000, oval BA was the dominant spot in its latitude and in that sense it resembled more a miniature version of the GRS than a vortex street configuration. The analysis of the data corresponding to BA post-2000 reveals a statistically significant period of oscillation at 138 days with a peak-to-peak amplitude of 1.2 degrees. Based on different data of BA from 2000 to 2008 García-Melendo et al. (2009) reported a period for BA's longitudinal position of about 159 days, which is approximately the same as the 158 days period that we found for the WOS prior to 2000, but is longer than the 138 days period that we found for oval BA. For comparison, Figure 11 shows the periodogram analysis of the JUPOS BA data between the years 2000 and 2008. When limiting the signal to those years, the periodogram analysis becomes more sensitive to Jupiter's synodic period, and thus the aliases of the main peak with this period are relative higher than when the signal is longer. However, the main period we found in this case is closer to the value reported by García-Melendo et al. (2009).

4.3. Nature of the Oscillations

Historically, several different hypotheses have been proposed to explain the nature of the GRS's longitudinal oscillation. One possible explanation would be that the spot is reacting to changes in the background zonal flow. Ingersoll and Cuong (1981) showed

that the GRS can be understood as a quasi-geostrophic (QG) vortex that can maintain itself by absorbing smaller eddies. In this QG framework, if unperturbed by nearby spots or waves, finite vortices would tend to move with the local zonal velocity averaged over their area (Marcus 1988, 1993; Marcus and Lee 1994). **Therefore, if the zonal profile is stable, the observed oscillations in longitudinal position could be associated with oscillations in the spot's area, or with variations of its latitudinal position with respect to the zonal profile, or both.** The spectral analysis of these variables derived from the data in the JUPOS database does not reveal any statistically significant peak. Observations with higher resolution and cadence would be necessary to detect such oscillations.

Another alternative to explain the oscillations could be that the spot oscillates because it interacts with other nearby features. In the QG framework, the drift of a finite vortex can be also affected by the velocities created by other nearby vorticity patches (Youssef and Marcus 2003). The GRS experiences close encounters with other features periodically. For example, the GRS and the oval BA pass nearby each other approximately every two years ($\approx$ 742 days), and recent BA data shows it clearly speeds up during a passage and then slows back down, for example in 2008 (Sanchez-Lavega et al. 2013). Recent observations have also revealed how the GRS oscillation period can be disrupted by interactions with nearby features (Sánchez-Lavega et al. 2021). Numerical simulations have also shown that oscillations can be caused by wave-spot interactions (Williams 1997).

Finally, another possibility could be that different vertical levels of the vortex interact with each other in a way that they produce oscillations. Achterberg and Ingersoll (1994) using an f-plane model, showed that internal barotropic instability, in the presence of a zonal shear, could cause latitudinal and longitudinal oscillations of a vortex leading to its vertical fragmentation. In their model, the vortices' longitudinal oscillations have a larger

amplitude than their latitudinal oscillations and in general these increase with time. When the amplitude of the oscillations becomes sufficiently large (approximately the radius of the vortex), the spot would separate vertically and the upper and lower part of the vortex would be advected by the zonal flow. However, this would only be applicable for vortices smaller than the deformation radius, which on Jupiter is estimated to be between 1,500 and 2,000 km in the latitudinal region occupied by the GRS and the WOS (Read et al. 2006). **Thus it is unlikely that this is the mechanism causing the observed oscillations in the GRS and oval BA described in this paper.**

5. Conclusions

We have used the data recorded in the JUPOS data base relative to the GRS and the WOS to retrieve information about their drift, size and location over time. The analysis of the longitudinal positions of the spots confirms that the historical period and amplitude of oscillation of the GRS in longitude continues being stable despite the changes in size **and maximum peripheral velocity**. The analysis of the data for the WOS prior to the year 2000 **seems to show evidence of oscillations in longitude similar in peak-to-peak amplitude to those of the GRS but with longer periods.** Finally, the analysis of the data corresponding to oval BA, reveals a statistically significant period of oscillation at 138 days with a peak-to-peak amplitude of 1.2 degrees. **Once again, the amplitude of this oscillation is similar to that reported in a previous study,** García-Melendo et al. (2009) **but the period is smaller.**

The analysis of the data in the JUPOS database did not allow us to discern if the longitudinal oscillations were correlated with oscillations in the spots' sizes or latitudinal locations, and thus the cause of these oscillations remains an unsolved problem. Characterizing possible correlations in order to determine a plausible cause for the

oscillations, and determining if the period of oscillation of BA is decreasing would require high cadence and resolution campaigns to monitor the evolution of these spots over time. In the meanwhile, more sophisticated numerical modeling can be conducted to investigate the nature of vortex oscillations.

Acknowledgments:

We are grateful to Hans-Joerg Mettig and the JUPOS team. This work used data acquired from the NASA/ESA HST Space Telescope, associated with programs: GO10192, GO10783, GO11096, GO11498, GO13067, GO13937, GO14334, GO14756, GO15262, GO15502, and GO15929, with support provided to AAS by the Space Telescope Science Institute, which is operated by the Association of Universities for Research in Astronomy, Inc., under NASA contract NAS 5-26555. We are also thankful to the anonymous referees for their comments.

A. Jupiter Radius and Latitude Systems

Resolution B3 of the XXIXth International Astronomical Union General Assembly recommends using the values $R_e = 71,492$ km and $R_p = 66,854$ km for the equatorial and polar radius of Jupiter. With these values, the volumetric mean radius (which is the radius of the sphere with the same volume as Jupiter) can be calculated as $(Re^2Rp)^{1/3}$ = 69,911 km.

For oblate spheroids (like Jupiter) there are two possible ways to define the latitude. The *planetocentric* latitude (λ_c) is the latitude referenced to the center of the planet. The *planetographic* latitude (λ_g) is the latitude referenced to a line directed along the local vertical. The conversion between these two different latitudes can be given as a function of the ratio of the equatorial to the polar radius as follows:

$$\tan(\lambda_g) = \left(\frac{R_e}{R_p}\right)^2 \tan(\lambda_c) \tag{A1}$$

With these definitions the value of the radius at a given λ_c will be given by:

$$R(\lambda_c) = \frac{R_e R_p}{\sqrt{R_e^2 \sin^2(\lambda_c) + R_p^2 \sin^2(\lambda_c)}} \tag{A2}$$

At the locations of the GRS ($\lambda_g \approx 22$ degrees south) and the WOS ($\lambda_g \approx 30$ degrees south) the radius estimated this way would be $70,929$ km and $70,472$ km respectively.

B. Systems of Longitude

Jupiter has three IAU recognized rotation periods. Namely, System I with a period of 9h 50m and 30.0034s, System II with a period of 9h 55m and 40.6322s, and System III with a period of 9h 55m and 29.37s. System I and System II are derived from the average translation rate of features in the equator and of the GRS respectively. System III is based on the period of the recurring decametric radiation bursts and it is the current standard system (Riddle and Warwick 1976; Dessler 1983).

The longitude in System III can be computed as follows:

$$L_{III}(t) = 217.956^\circ + 870.536(t - t_0) \tag{B1}$$

where $L(t)$ is the longitude at a given time t, and $t - t_0$ is the time in days elapsed since 0^h UT Jan. 1, 1965. The conversion between System II and System III longitude is given by:

$$L_{III}(t) = L_{II}(t) + 81.245 + 0.266(t - t_0) \tag{B2}$$

REFERENCES

Achterberg, R.K., Ingersoll, A.P., 1994. Numerical simulation of baroclinic Jovian vortices. Journal of Atmospheric Sciences 51, 541–562. doi:10.1175/1520-0469(1994)051<0541:NSOBJV>2.0.CO;2.

Baluev, R.V., 2008. Assessing the statistical significance of periodogram peaks. MNRAS 385, 1279–1285. doi:10.1111/j.1365-2966.2008.12689.x, arXiv:0711.0330.

Cosentino, R.G., Butler, B., Sault, B., Morales-Juberías, R., Simon, A., de Pater, I., 2017. Atmospheric waves and dynamics beneath Jupiter's clouds from radio wavelength observations. Icarus 292, 168–181. doi:10.1016/j.icarus.2017.01.006, arXiv:1701.03484.

Denning, W.F., 1885. The Red Spot on Jupiter. Nature 32, 626. doi:10.1038/032626a0.

Dessler, A.J., 1983. Coordinate systems. pp. 498–504.

García-Melendo, E., Legarreta, J., Sánchez-Lavega, A., Hueso, R., Pérez-Hoyos, S., González, J., Gómez-Forrellad, J.M., IOPW Team, 2009. The jovian anticyclone BA. I. Motions and interaction with the GRS from observations and non-linear simulations. Icarus 203, 486–498. doi:10.1016/j.icarus.2009.05.031.

Guitar, H., 1984. Analysis of motions of Jupiter's Great Red Spot and White Ovals. PhD Thesis, New Mexico State University. .

Humphreys, T., Marcus, P.S., 2007. Vortex Street Dynamics: The Selection Mechanism for the Areas and Locations of Jupiter's Vortices. Journal of Atmospheric Sciences 64, 1318–+. doi:10.1175/JAS3882.1.

Ingersoll, A.P., Cuong, P.G., 1981. Numerical model of long-lived Jovian vortices. Journal of Atmospheric Sciences 38, 2067–2076. doi:10.1175/1520-0469(1981)038.

Hans Jorg Mettig, Grischa Hahn, 1995. Jupos Database for object positions on Jupiter, in: Hans Jorg Mettig, Grischa Hahn (Eds.), Project Documentation, pp. 1 – 26. URL: http://www.jupos.org/etc/JuposProjDoc_English.pdf.

Kardasis, E., Rogers, J.H., Orton, G., Delcroix, M., Christou, A., Foulkes, M., Yanamandra-Fisher, P., Jacquesson, M., Maravelias, G., 2016. The need for professional-amateur collaboration in studies of Jupiter and Saturn. Journal of the British Astronomical Association 126, 29–39. arXiv:1503.07878.

Lomb, N.R., 1976. Least-Squares Frequency Analysis of Unequally Spaced Data. Ap&SS 39, 447–462. doi:10.1007/BF00648343.

Marcus, P.S., 1988. Numerical simulation of Jupiter's Great Red Spot. Nature 331, 693–696. doi:10.1038/331693a0.

Marcus, P.S., 1993. Jupiter's Great Red Spot and other vortices. Annual review of Astronomy and Astrophysics 31, 523–573. doi:10.1146/annurev.aa.31.090193.002515.

Marcus, P.S., Asay-Davis, X., Wong, M.H., de Pater, I., 2012. Jupiters Red Oval BA: Dynamics, Color, and Relationship to Jovian Climate Change. Journal of Heat Transfer 135. URL: https://doi.org/10.1115/1.4007666, doi:10.1115/1.4007666, arXiv:https://asmedigitalcollection.asme.org/heattransfer/article-pdf/135/1/011007 011007.

Marcus, P.S., Lee, C., 1994. Jupiter's Great Red Spot and zonal winds as a self-consistent, one-layer, quasigeostrophic flow. Chaos 4, 269–286. doi:10.1063/1.166007.

Wes McKinney, 2010. Data Structures for Statistical Computing in Python, in: Stéfan van der Walt, Jarrod Millman (Eds.), Proceedings of the 9th Python in Science Conference, pp. 56 – 61. doi:10.25080/Majora-92bf1922-00a.

Morales-Juberías, R., Brindle, E.S., Dowling, T.E., 2010. Jupiter's South South Temperate Zone vortices: Observations and simulations. Icarus 206, 747–754. doi:10.1016/j.icarus.2009.10.002.

Morales-Juberías, R., Sánchez-Lavega, A., Dowling, T.E., 2003. EPIC simulations of the merger of Jupiter's White Ovals BE and FA: altitude-dependent behavior. Icarus 166, 63–74. doi:10.1016/S0019-1035(03)00259-8.

Morales-Juberías, R., Sánchez-Lavega, A., Lecacheux, J., Colas, F., 2002. A Comparative Study of Jovian Anticyclone Properties from a Six-Year (1994-2000) Survey. Icarus 157, 76–90. doi:10.1006/icar.2001.6819.

Peek, B.M., 1958. The Planet Jupiter. Faber and Faber, pp. 240. ISBN 0571180264. Rev. ed., 1981.

Pérez-Hoyos, S., Sánchez-Lavega, A., Hueso, R., García-Melendo, E., Legarreta, J., 2009. The jovian anticyclone BA. III. Aerosol properties and color change. Icarus 203, 516–530. doi:10.1016/j.icarus.2009.06.024.

Press, W.H., Rybicki, G.B., 1989. Fast Algorithm for Spectral Analysis of Unevenly Sampled Data. ApJ 338, 277. doi:10.1086/167197.

Read, P.L., Gierasch, P.J., Conrath, B.J., Simon-Miller, A., Fouchet, T., Yamazaki, Y.H., 2006. Mapping potential-vorticity dynamics on Jupiter. I: Zonal-mean circulation from Cassini and Voyager 1 data. Quarterly Journal of the Royal Meteorological Society 132, 1577–1603.

Reese, E.J., 1972. Jupiter: Its Red Spot and Disturbances in 1970-1971. Icarus 17, 57–72. doi:10.1016/0019-1035(72)90046-2.

Riddle, A.C., Warwick, J.W., 1976. Redefinition of System III longitude. Icarus 27, 457–459. doi:10.1016/0019-1035(76)90025-7.

Rogers, J.H., 1995. The giant planet Jupiter. Practical Astronomy Handbooks, Cambridge: University Press, —c1995.

Rogers, J.H., 2008. The accelerating circulation of Jupiter's Great Red Spot. Journal of the British Astronomical Association 118, 14–20.

Sánchez-Lavega, A., Anguiano-Arteaga, A., Iñurrigarro, P., Garcia-Melendo, E., Legarreta, J., Hueso, R., Sanz-Requena, J.F., Pérez-Hoyos, S., Mendikoa, I., Soria, M., Rojas, J.F., Andrés-Carcasona, M., Prat-Gasull, A., Ordoñez-Extebarria, I., Rogers, J.H., Foster, C., Mizumoto, S., Casely, A., Hansen, C.J., Orton, G.S., Momary, T., Eichstädt, G., 2021. Jupiter's Great Red Spot: Strong Interactions With Incoming Anticyclones in 2019. Journal of Geophysical Research (Planets) 126, e06686. doi:10.1029/2020JE006686.

Sanchez-Lavega, A., Legarreta, J., Garca-Melendo, E., Hueso, R., Perez-Hoyos, S., Gomez-Forrellad, J.M., Fletcher, L.N., Orton, G.S., Simon-Miller, A., Chanover, N., Irwin, P., Tanga, P., Cecconi, M., 2013. Colors of jupiter's large anticyclones and the interaction of a tropical red oval with the great red spot in 2008. Journal of Geophysical Research: Planets 118, 2537–2557. URL: https://agupubs.onlinelibrary.wiley.com/doi/abs/10.1002/2013JE004371, doi:https://doi.org/10.1002/2013JE004371, arXiv:https://agupubs.onlinelibrary.wiley.com/doi/pdf/10.1002/2013JE004371.

Sanchez-Lavega, A., Orton, G.S., Morales, R., Lecacheux, J., Colas, F., Fisher, B., Fukumura-Sawada, P., Golisch, W., Griep, D., Kaminski, C., Baines, K., Rages, K.,

West, R., 2001. NOTE: The Merger of Two Giant Anticyclones in the Atmosphere of Jupiter. Icarus 149, 491–495. doi:10.1006/icar.2000.6548.

Sánchez-Lavega, A., Rojas, J.F., Hueso, R., Lecacheux, J., Colas, F., Acarreta, J.R., Miyazaki, I., Parker, D., 1999. Interaction of Jovian White Ovals BC and DE in 1998 from Earth-Based Observations in the Visual Range. Icarus 142, 116–124. doi:10.1006/icar.1999.6197.

Scargle, J.D., 1982. Studies in astronomical time series analysis. II. Statistical aspects of spectral analysis of unevenly spaced data. ApJ 263, 835–853. doi:10.1086/160554.

Simon, A.A., Beebe, R.F., 1996. Jovian Tropospheric Features — Wind Field, Morphology, and Motion of Long-Lived Systems. Icarus 121, 319–330. doi:10.1006/icar.1996.0090.

Simon, A.A., Beebe, R.F., Gierasch, P.J., Vasavada, A.R., Belton, M.J.S., 1998. Global Context of the Galileo-E6 Observations of Jupiter's White Ovals. Icarus 135, 220–229. doi:10.1006/icar.1998.5970.

Simon, A.A., Tabataba-Vakili, F., Cosentino, R., Beebe, R.F., Wong, M.H., Orton, G.S., 2018. Historical and Contemporary Trends in the Size, Drift, and Color of Jupiter's Great Red Spot. AJ 155, 151. doi:10.3847/1538-3881/aaae01.

Simon, A.A., Wong, M.H., Rogers, J.H., Orton, G.S., de Pater, I., Asay-Davis, X., Carlson, R.W., Marcus, P.S., 2014. Dramatic Change in Jupiter's Great Red Spot from Spacecraft Observations. The Astrophysical Journal 797, L31. URL: https://doi.org/10.1088/2041-8205/797/2/131, doi:10.1088/2041-8205/797/2/131.

Simon-Miller, A.A., Chanover, N.J., Orton, G.S., Sussman, M., Tsavaris, I.G., Karkoschka, E., 2006. Jupiter's White Oval turns red. Icarus 185, 558–562. doi:10.1016/j.icarus.2006.08.002.

Simon-Miller, A.A., Gierasch, P.J., Beebe, R.F., Conrath, B., Flasar, F.M., Achterberg, R.K., Cassini CIRS Team, 2002. New Observational Results Concerning Jupiter's Great Red Spot. Icarus 158, 249–266. doi:10.1006/icar.2002.6867.

Solberg, H.G., 1969. A 3-month oscillation in the longitude of Jupiter's red spot. Planet. Space Sci. 17, 1573–1580. doi:10.1016/0032-0633(69)90146-9.

Reback J. & The pandas development team, 2020. pandas, Zenodo. URL: https://doi.org/10.5281/zenodo.3509134, doi:10.5281/zenodo.3509134.

Trigo-Rodriguez, J.M., Sánchez-Lavega, A., Gómez, J.M., Lecacheux, J., Colas, F., Miyazaki, I., 2000. The 90-day oscillations of Jupiter's Great Red Spot revisited. Planetary and Space Sciences 48, 331–339.

Vanderplas, J., 2015. gatspy: General tools for Astronomical Time Series in Python. URL: https://doi.org/10.5281/zenodo.14833, doi:10.5281/zenodo.14833.

VanderPlas, J.T., 2018. Understanding the Lomb-Scargle Periodogram. ApJS 236, 16. doi:10.3847/1538-4365/aab766, arXiv:1703.09824.

VanderPlas, J.T., Ivezić, Ž., 2015. Periodograms for Multiband Astronomical Time Series. ApJ 812, 18. doi:10.1088/0004-637X/812/1/18, arXiv:1502.01344.

Williams, G.P., 1997. Planetary vortices and Jupiter's vertical structure. Journal of Geophysical Research 102, 9303–9308. doi:10.1029/97JE00520.

Wong, M.H., de Pater, I., Asay-Davis, X., Marcus, P.S., Go, C.Y., 2011. Vertical structure of Jupiter's Oval BA before and after it reddened: What changed? Icarus 215, 211–225. doi:10.1016/j.icarus.2011.06.032.

Youssef, A., Marcus, P.S., 2003. The dynamics of jovian white ovals from formation to merger. Icarus 162, 74–93. doi:10.1016/S0019-1035(02)00060-X.

This manuscript was prepared with the AAS LaTeX macros v5.2.

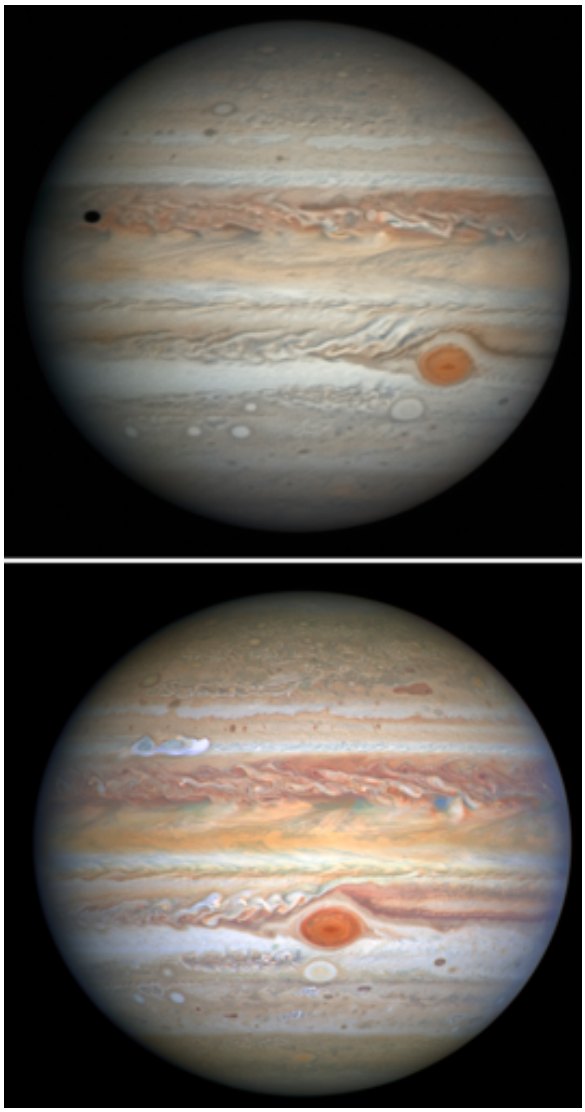

Fig. 1.— Top: Color view of Jupiter on Aug. 18, 2020 (Damian Peach) ; Bottom: HST-OPAL enhanced color view of Jupiter on Aug. 25, 2020

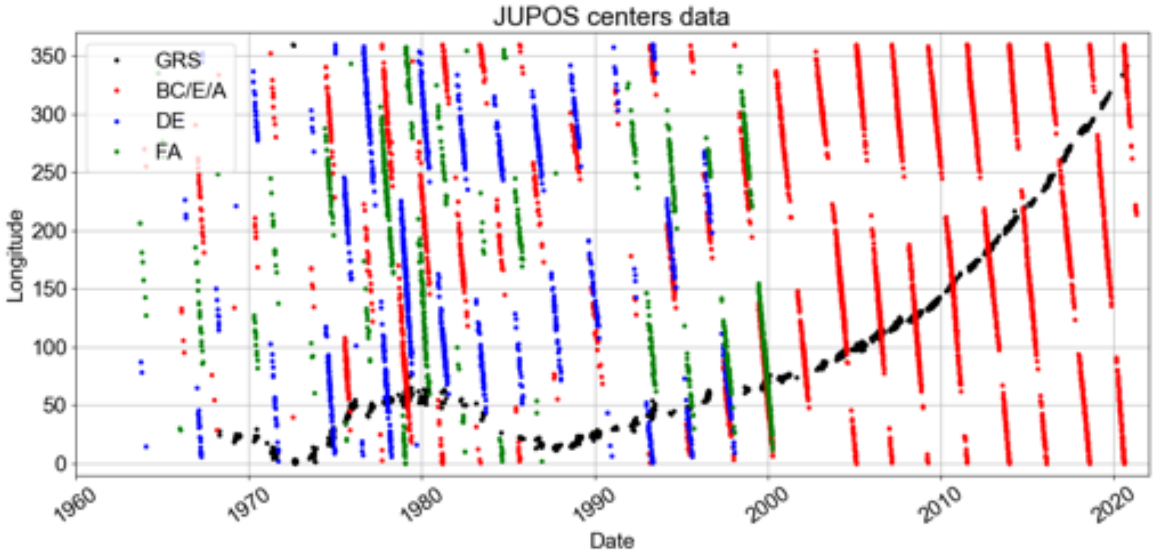

Fig. 2.— System II longitude of the center of the GRS and the WOS recorded in the JUPOS database.

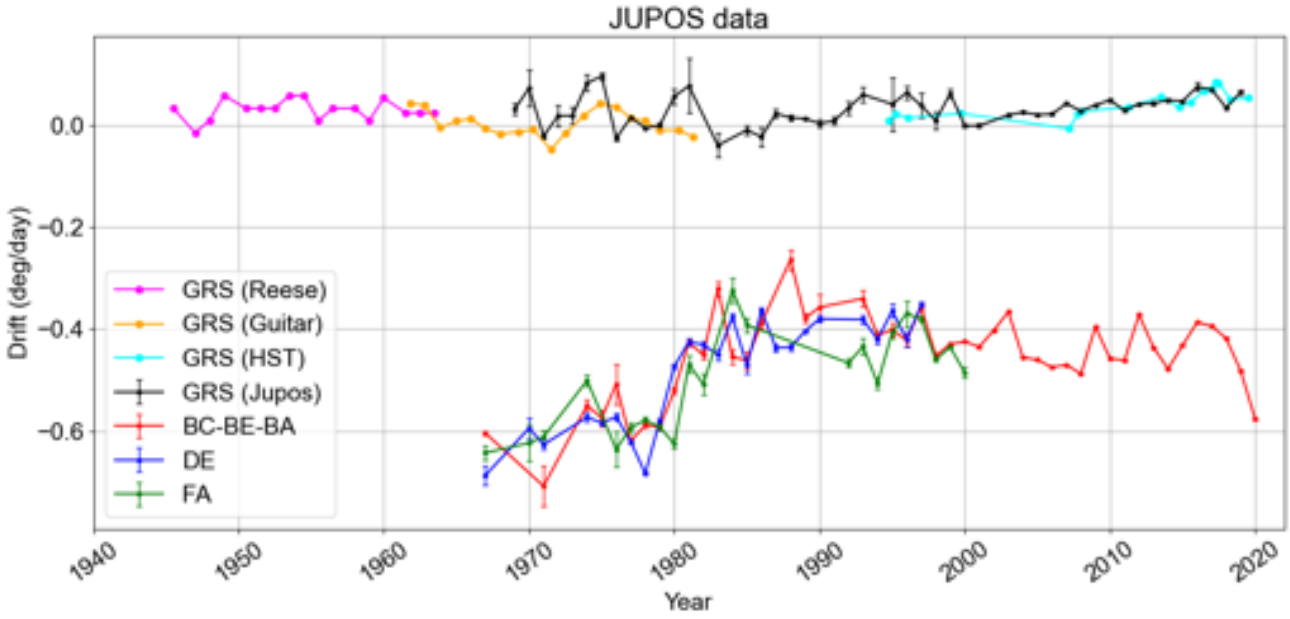

Fig. 3.— Annual System II drift rate of the GRS and the WOS in degrees per day derived from linear fits to the annual longitude data in the JUPOS database. For context we also show the data from Reese, Guitar, and HST (Simon et al. 2018) transformed to System II using a system of reference shift given by $D_{II} = D_{III} - 0.266$, where D_{II} and D_{III} are the drift rates in system II and III respectively.

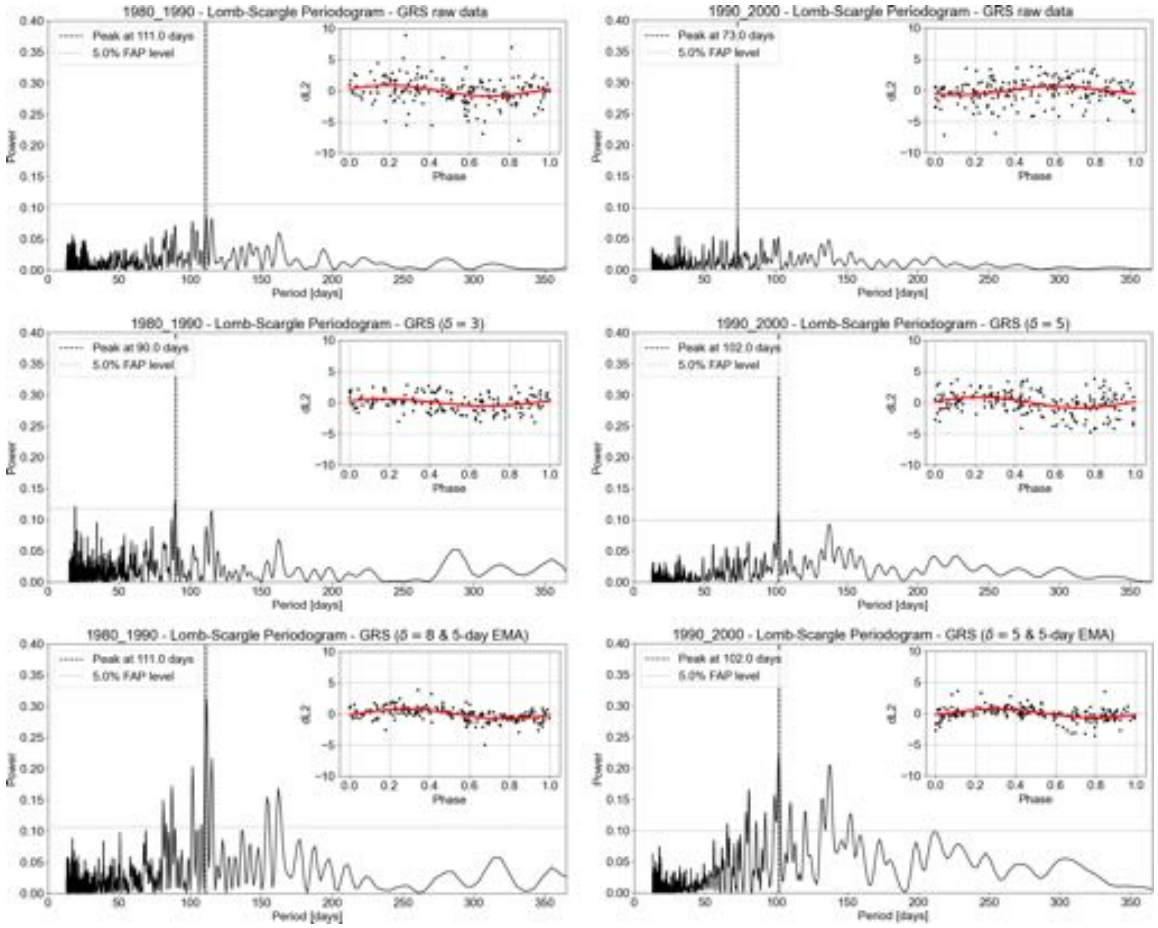

Fig. 4.— **Lomb-Scargle periodogram of GRS System II longitude detrended data (dL2) corresponding the 80s (left) and 90s (right). The embedded plots show the phase curve of the data with the fit to the corresponding period. The top panels show the periodogram of the raw series. The middle panels show the periodograms of the data after removing points that deviate δ degrees from the detrended mean. The bottom panels show the periodograms of the data after removing points that deviate δ degrees from the detrended mean and using a 5-day exponential moving average.**

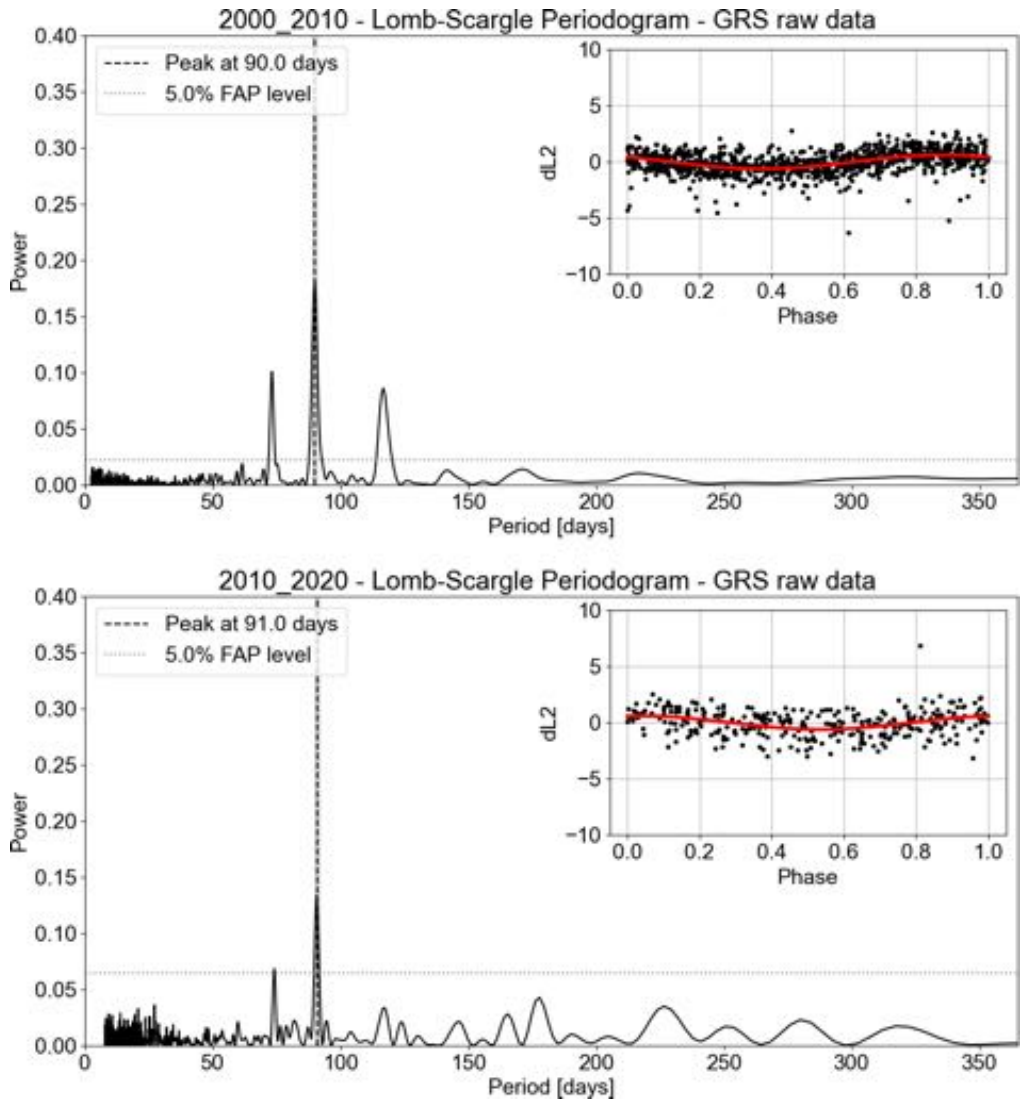

Fig. 5.— **Lomb-Scargle periodogram of GRS System II longitude detrended raw data (dL2) for the 2000s (Top) and 2010s (Bottom). The embedded plots show the phase curve of the data with the fit to the corresponding period.**

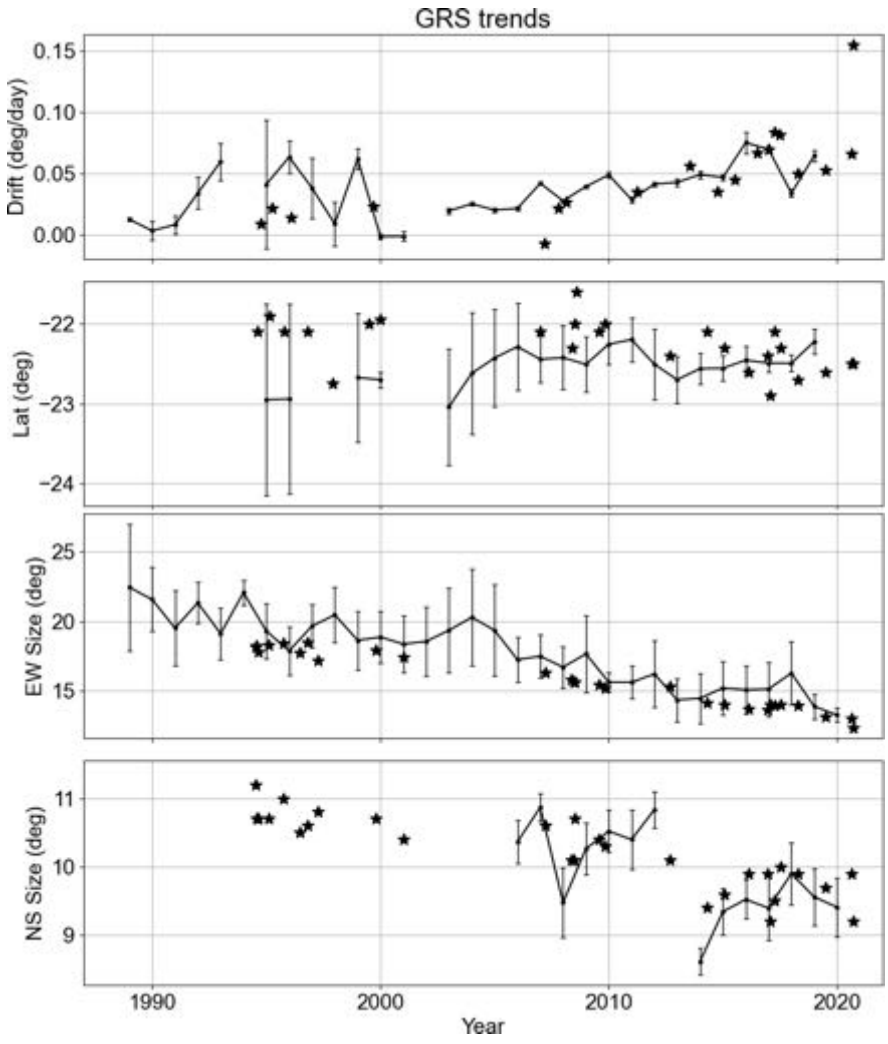

Fig. 6.— Change of the GRS annual drift rate (top panel), latitudinal position (second panel), zonal size (third panel) and meridional size (bottom panel) as a function of time. The stars represent measurements based on HST images (Simon et al. 2018). **The North or South positions of the spots have been recorded just sporadically in the JUPOS database, which explain the gaps seen in the bottom panel.**

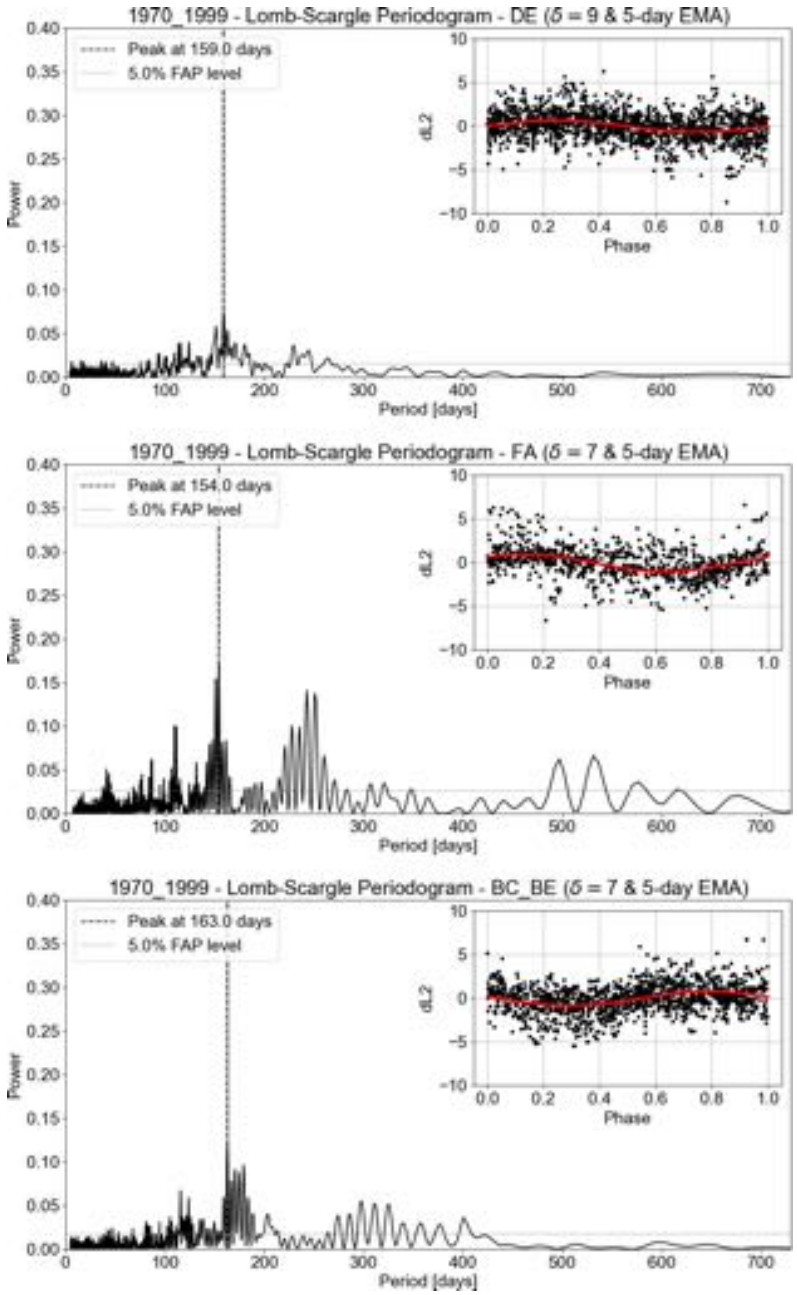

Fig. 7.— **Lomb-Scargle periodogram** of the WOS longitude detrended and filtered data (dL2) corresponding the years 1970-1999. **The inside panel shows the phase curve corresponding to the highest period in the power spectra.**

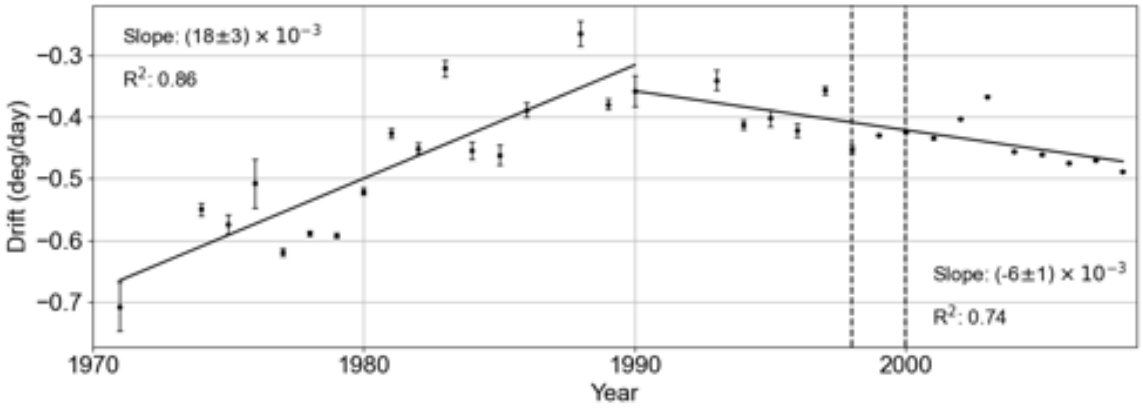

Fig. 8.— **Linear fits to the BC/BE/BA data between 1971 and 2008. The vertical dashed lines mark the years of the mergers between the ovals BC & DE (1997) and BE & FA (2000).**

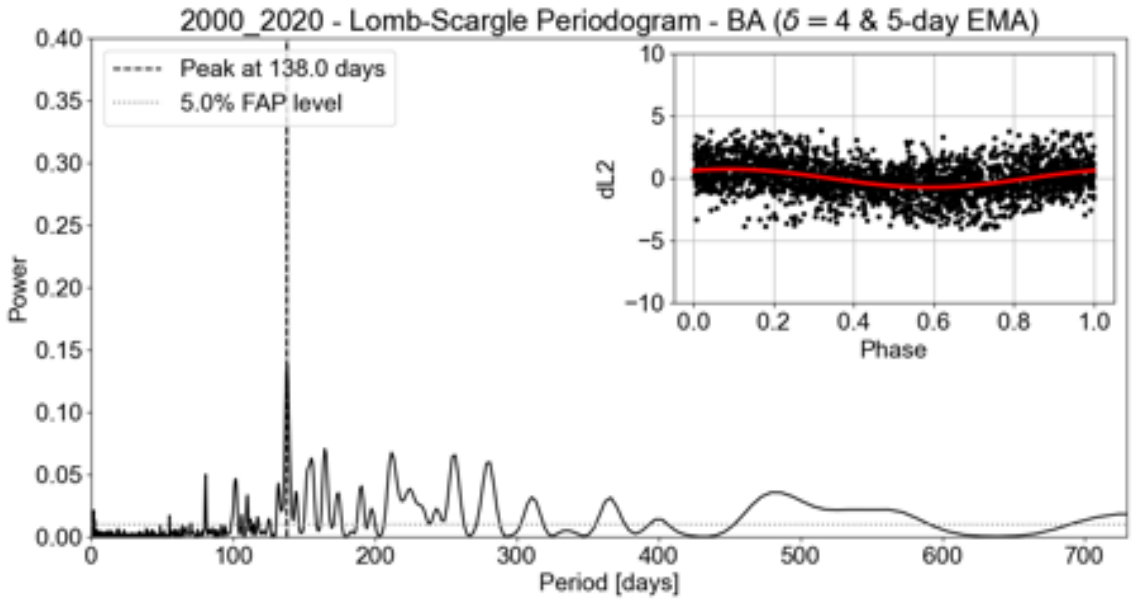

Fig. 9.— **Lomb-Scargle periodogram** of oval BA longitude detrended and filtered data (dL2) corresponding the years 2000-2020. **The inside panel shows the phase curve corresponding to the highest period in the power spectra.**

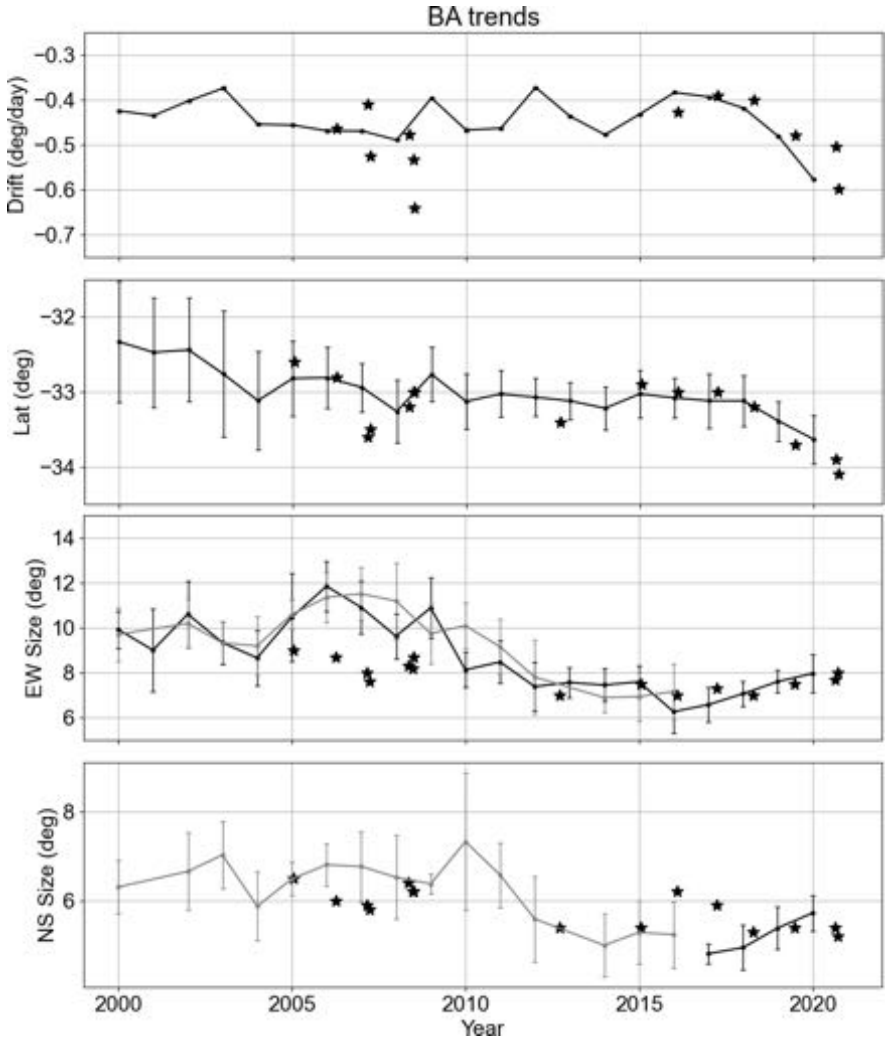

Fig. 10.— Change of BA **annual drift rate (top panel), latitudinal position (second panel), zonal size (third panel) and meridional size (bottom panel) as a function of time. In all the panels the stars represent measurements from HST data. In the two bottom panels the gray data points and lines show additional measurements made to fill in the gaps in the JUPOS database.**

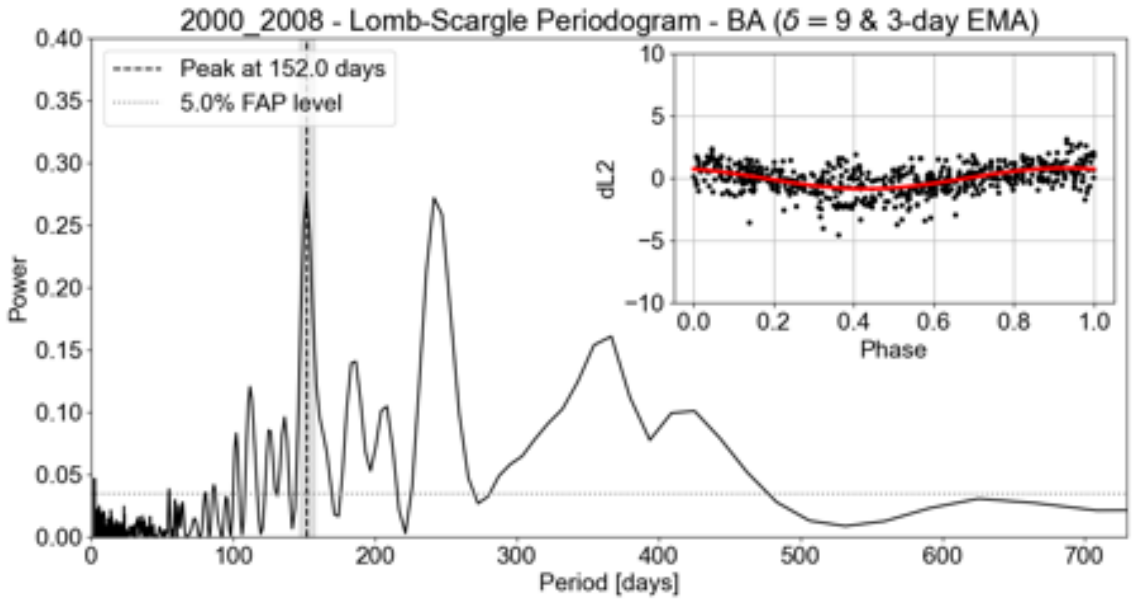

Fig. 11.— **Lomb-Scargle periodogram** of oval BA longitude detrended and filtered data (dL2) corresponding the years 2000-2008. **The inside panel shows the phase curve corresponding to the highest period in the power spectra.**

Table 1: GRS oscillation data. The brackets around the periods and amplitudes indicate peaks that were under or close to the 5% FAP level.

Reference	Years	LII points	P(days)	Amp. (°)	Lat (°)
Reese (1972)	1970-1971		89.89	1.54	-22.5 ± 0.5
Guitar (1984)	1961-1981		89.93	1.06	-22.5 ± 0.5
Trigo-Rodriguez et al. (2000)	1993-1999	317	89.8	1.2	-22.3 ± 0.6
Rogers (2008)	2000-2005		90	1.0	-22.4 ± 0.2
JUPOS raw		193	(111)	(1.8)	
JUPOS ($\delta = 3$)	1980s	169	(90)	(1.2)	-22.6 ± 0.6
JUPOS ($\delta = 8$ & 5 day EMA)		192	111	1.6	
JUPOS raw		210	(73)	(1.4)	
JUPOS ($\delta = 5$)	1990s	207	(102)	(1.8)	-22.8 ± 0.2
JUPOS ($\delta = 5$ & 5 day EMA)		207	102	1.4	
JUPOS raw	2000s	1055	90	1.2	-22.7 ± 0.7
JUPOS raw	2010s	326	91	1.2	-22.4 ± 0.2

Table 2: WOS oscillation data.

Oval Name (filtering parameters)	Years	LII points	P(days)	Amp. (°)	Lat (°)
DE ($\delta = 9$ & 5 day EMA)	1970-1999	1,619	159	1.4	-34.1 ± 0.9
FA ($\delta = 7$ & 5 day EMA)	1970-1999	923	154	2.0	-33 ± 1
BC/BE ($\delta = 7$ & 5 day EMA)	1970-1999	1,396	163	1.6	-33.3 ± 0.8
BA (García-Melendo et al. 2009)	2000-2008		157 ± 10	1.2	≈ -33
BA ($\delta = 4$ & 5 day EMA)	2000-2020	2,692	138	1.4	-33.1 ± 0.2